ARMY RESEARCH LABORATORY

Inductance Scaling of a Helicoil Using ALEGRA

by Robert Doney

ARL-TR-6397 May 2013

NOTICES

Disclaimers

The findings in this report are not to be construed as an official Department of the Army position unless so designated by other authorized documents.

Citation of manufacturer's or trade names does not constitute an official endorsement or approval of the use thereof.

Destroy this report when it is no longer needed. Do not return it to the originator.

Army Research Laboratory

Aberdeen Proving Ground, MD 21005-5066

ARL-TR-6397 **May 2013**

Inductance Scaling of a Helicoil Using ALEGRA

Robert Doney

Weapons and Materials Research Directorate, ARL

REPORT DOCUMENTATION PAGE	Form Approved OMB No. 0704-0188

1. REPORT DATE *(DD-MM-YYYY)*	2. REPORT TYPE	3. DATES COVERED (From - To)
May 2013	Final	January 2011-January 2012

4. TITLE AND SUBTITLE
Inductance Scaling of a Helicoil Using ALEGRA

5a. CONTRACT NUMBER

5b. GRANT NUMBER

5c. PROGRAM ELEMENT NUMBER

6. AUTHOR(S)
Robert Doney

5d. PROJECT NUMBER

5e. TASK NUMBER

5f. WORK UNIT NUMBER

7. PERFORMING ORGANIZATION NAME(S) AND ADDRESS(ES)
U.S. Army Research Laboratory
ATTN: RDRL-WMP-D
Aberdeen Proving Ground, MD 21005-5066

8. PERFORMING ORGANIZATION REPORT NUMBER
ARL-TR-6397

9. SPONSORING/MONITORING AGENCY NAME(S) AND ADDRESS(ES)

10. SPONSOR/MONITOR'S ACRONYM(S)

11. SPONSOR/MONITOR'S REPORT NUMBER(S)

12. DISTRIBUTION/AVAILABILITY STATEMENT
Approved for public release; distribution is unlimited.

13. SUPPLEMENTARY NOTES

14. ABSTRACT
The inductance scaling of several helicoil configurations are investigated using the March 2011 release of the Sandia magnetohydrodynamics (MHD) code, ALEGRA. A great majority of the effort is spent ensuring proper convergence of relevant variables for an accurate solution, such as mesh size, resolution, grid biasing, and solver tolerance. For these helicoil geometries, steady-state magnetic diffusion time requires several tens of milliseconds, up to two orders of magnitude greater than that required for coaxial conductors. Inductances are shown to scale quadratically with the number of conductor turns. At moderate to large N, results are in agreement with data provided by Bartkowski and Berning as well inductance calculated for a simple solenoid—a function of the number of turns squared. Surprisingly, the gap size between conducting turns had a minor impact on the results.

15. SUBJECT TERMS
ALEGRA, inductance, helicoil

16. SECURITY CLASSIFICATION OF:			17. LIMITATION OF ABSTRACT	18. NUMBER OF PAGES	19a. NAME OF RESPONSIBLE PERSON
a. REPORT	b. ABSTRACT	c. THIS PAGE			Robert Doney
Unclassified	Unclassified	Unclassified	UU	50	19b. TELEPHONE NUMBER (*Include area code*) 410-278-7309

Contents

List of Figures

Acknowledgment

I would like to thank Dr. Sikhanda Satapathy for his critical review of this manuscript and for proving important feedback. I'm also indebted to Dr. John Niederhaus at Sandia National Laboratories for his ongoing collaboration in related areas and outstanding technical support with ALEGRA. Mr. Peter Bartkowski and Dr. Paul Berning have also been strong collaborators and influential in this effort. I would also like to thank the Distributed Shared Resources Center at ERDC, part of the DoD High Performance Computing Modernization Program, for access to garnet to run these large calculations. Thanks go to Dr. Steven Segletes for his amazing work generating and keeping the LaTeX ARL template so that this report could be displayed at its best. Finally, I'd like to recognize the great editorial and publishing support from Ms. Lisa Lacey and Ms. Sherry Larson.

1. Introduction

Inductance, L, is an electric circuit property that is analogous to inertia or the resistance to change. Its value is determined by a geometry defined by the current path (*1*). When a voltage is suddenly applied to a circuit, electric current does not immediately jump to its intended value. Instead, it rises to that value in an amount of time proportional to the inductance. Similarly, when the voltage is removed, the current does not suddenly disappear—it also drops to zero in finite time. Inductors are specifically inserted into circuits for this type of timing control among other reasons. From a physics perspective, the work required to overcome this resistance to change can be thought of as putting magnetic energy into the system and is related to the inductance or the magnetic field, B, over some volume as,

$$E_m = \frac{1}{2} L I^2 = \frac{1}{2\mu_0} \int B^2 \, dV \tag{1}$$

where E_m is the magnetic energy, I is the current, and dV is the volume element. Through these relationships we are able to determine inductances and magnetic energies for simple geometries that helps one to understand their electrical response in time. This is important in countless applications since it is common to require a specific current profile. In most cases however, even seemingly simple geometries escape closed-form analytic expressions and must be evaluated through computational methods and approximations.

We are interested in measuring inductance for a complicated geometry known as the helicoil (figure 1a). As illustrated, we see a helical coil with a constant pitch and ten gap turns (or nine conducting turns). Also visible on the leftmost edge of figure 1a is a washer-type structure that connects the outer (helical) conductor with an inner smooth (return) conductor that is barely visible through the gaps in the coil. Figure 1b illustrates the device after rotation and coil visibility is turned off. At axial positions away from the coil, the device can be treated as a coaxial cable. An exact solution for the inductance is not possible since the current density in the return cap is not known and the coil section itself requires approximations. The deep history of various aspects of this problem is compelling with much effort spent on the elliptic integrals. The earliest records date back over one hundred years to the days of Lords Rayleigh and Kelvin (*2, 3*) with subsequent and substantial efforts by Rosa (*4*) and Grover (*5*). More recently (and with modern mathematical notation), relevant derivations have been performed by Knoepfel (*6, 7*), Turner (*8*), and Bartkowski (*9*). In this work, I am unable to consider short diffusion times (current on the surface) since it requires resolving the skin depth rather than the conductor

thickness. As the convergence analysis will show, the computational cost would be prohibitive. If one only considers the coaxial section, inductance is more easily calculated. It should be noted that the inductance depends on the amount of time allowed for the current to diffuse into the conductor. In many textbooks, the derivation proceeds by assuming that current only resides on the conductor's surface so that only the field between conductors is calculated. In this study full diffusion is considered so that after a sufficient amount of time, current is uniformly distributed through the thickness of the conductors. Therefore magnetic energy is tallied in each of the conductors and the gap between them. In this report, the inductance scaling of several helicoil configurations are investigated using the March 2011 release of the Sandia magnetohydrodynamics (MHD) code, ALEGRA. Several hundred thousand core hours of simulations were run on Garnet, a Cray XE-6 located at the U.S. Army Engineer Research and Development Center. This report is organized in the following manner. Section 2 discusses relevant preliminaries and the computational setup—some details on coaxial conductors and magnetic diffusion are considered. Section 3 provides the inductance scaling as well as a quadratic fit which is approximately equivalent for $1/8$-, $1/4$-, and $3/8$-inch air gaps.

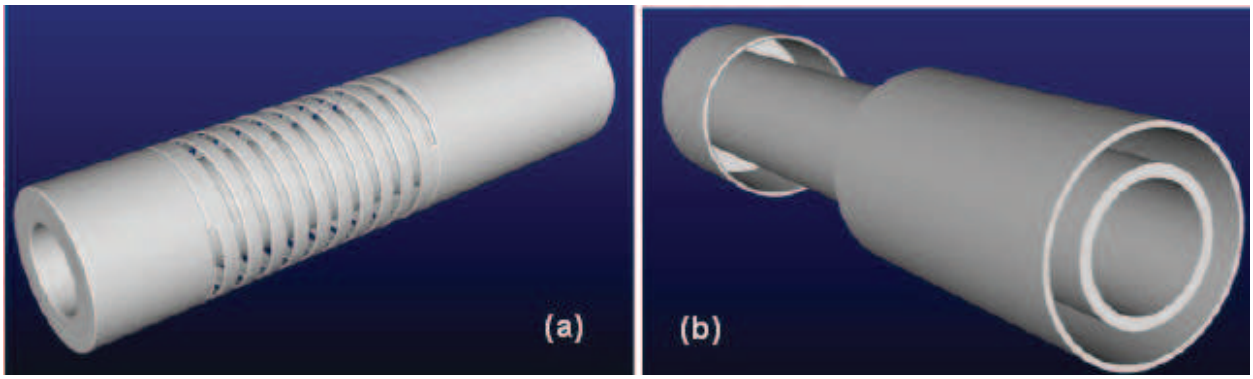

Figure 1. (a) Helicoil with ten gap turns (or nine conducting turns) and a constant pitch. (b) Opposite end of the same device and with coil visibility turned off. The inner and outer conductors are clearly visible and form a coaxial cable.

2. Preliminaries and Computational Setup

Since the coil is bounded axially by coaxial cylinder sections, it is helpful to first discuss the inductance and diffusion of a coaxial cable. To further simplify the problem, the return cap can be eliminated by extending the conductors from one side of the mesh to the other, axially. Current return is then handled by the boundary conditions. The inductance for this problem has

an analytic solution, which is derived in appendix A. Niederhaus has documented a verification study for the problem and shown that ALEGRA agrees to within 0.1% of theory (*10*). The bulk of the magnetic energy is stored between the conductors.

Following Jackson's analysis (*11*), an order of magnitude relation for the magnetic diffusion time, τ, in a conductor can be obtained by considering the magnetic diffusion equation,

$$\nabla^2 B = \mu\sigma\frac{\partial B}{\partial t}. \tag{2}$$

The coaxial cable is azimuthally symmetric and invariant along z, so that in cylindrical coordinates the Laplacian operator, ∇^2, reduces to one (radial) dimension,

$$\frac{\partial^2 B}{\partial \rho^2} + \frac{1}{\rho}\frac{\partial B}{\partial \rho}.$$

Since the denominator holds units of length squared, it is clear that $\nabla^2 = O(B/L^2)$ and $\frac{\partial B}{\partial t} = O(B/\tau)$, where L is a characteristic (radial) length over which the field diffuses and has dimensions of time. These yield,

$$\tau = O(\mu\sigma L^2). \tag{3}$$

In perfect conductors (i.e., superconductors) it takes an infinite amount of time for the field to diffuse so that all of the current resides on the surface. For an aluminum conductor with thicknesses, 1/8 and 1/4 inch, the characteristic diffusion times are about 440 and 1770 μs, respectively. For helicoils however, there are no symmetries. The full Laplacian must be considered. As a result, the diffusion time can increase markedly.

For this study, I use the Sandia National Laboratories Finite Element MHD code, ALEGRA. It couples Maxwell's equations with multimaterial solid dynamics in the MHD approximation, which ignores displacement currents (*12–14*). Based on our confidence from Niederhaus's validation work, we proceed with 3D simulations of the helicoil. In general, our geometry (figure 1) consists of two concentric, cylindrical shells connected at one end by a simple load so that current coming down either the inner or outer shell can return via that connection along the other cylindrical shell. On the outer conductor, we cut out a helix with the following characteristics: the number of conductor turns, $N_c = \{1, 2, .., 9\}$, and the axial gap between conducting turns (or slot gap), s={1/8, 1/4, 3/8 inch}. For each case, the pitch, p, remains constant. Pitch is defined

as the axial length of one full conducting loop or turn. Recall that the number of gap turns, $N_g = N_c + 1$. For these studies, the length of the full helicoil, L_h, is held fixed so that, $L_h = s + pN_g$. From this point on, N refers to the number of conducting turns (i.e., $N = N_c$). Due to the severe computational cost associated with $s = 1/8$ inch and small N—which will become clear during the convergence analysis—the $s = 1/8$-inch scope is limited to $4 \leq N \leq 9$. Additionally, for 3/8 inch, N is limited to less than seven because the thicker conducting lengths could cause the coil section to extend beyond its intended length. Algorithmic checks were not put in place to monitor this.

A constant 100 amp DC current is supplied via the boundary condition that jumps to steady state within a few compute cycles—a rate much faster than the diffusion time and the convergence time for inductance. The current is allowed to diffuse fully through the conductor thickness, thus the skin depth is equal to conductor thickness (something easy to resolve). A consequence of this is that field diffuses into the inner volume. This bypasses the shielding effect which is equivalent to the armature not being present (*15*). Other device dimensions are 4.5-inch outer diameter and 1/8-inch thickness for the outer conductor, and 3-inch outer diameter and 1/4-inch thickness for the inner conductor. Current feed (front), coil (middle), and return (back) lengths are 1.2, 0.2, and 0.08 m, respectively for a total device length of about 1.5 m.

The computational domain is defined by a radial trisection mesh consisting of five radial blocks or layers. Each block has a radius so that the 2nd and 4th blocks match the inner and outer conductor thicknesses, respectively. This is generally good practice and minimizes mixed cells and currents. The latter is not completely true however. Due to the numerical method and in order to preserve a divergence-free B (*16*), currents move around cell edges. Since each cell edge is shared by multiple cells (two in 2D and four in 3D), current will appear in each. This has ramifications for tallying current since tallies are commonly defined by sidesets and those are typically controlled by blocks. There is no easy way to extend them on a cell-by-cell basis, so relevant surface currents can be under-predicted. In time, as currents diffuse into the conductor, the tallied current approaches the expected current. If these details are critical, one can use advanced visualization tools, such as Ensight, to integrate the current density out to a radius that includes cells containing smeared current.

Before initiating the primary study, a substantial amount of convergence analysis is required to ensure an accurate solution. These details are outlined in appendix B. This amount of work actually exceeds that required for a seemingly simple inductance study! In contrast to the local behavior of solid mechanics calculations, MHD simulations deal in field quantities that extend to infinity—this means that domain size can affect the results. Additionally, more numeric solvers

(*17*) are employed each with their own tolerances. This is all in addition to the normal convergence analysis required for mesh resolution. Initially, I chose our convergence tolerance for relevant variables as 0.1%—meaning that, once subsequent refinement in a variable yielded a change that small, I considered it to be converged. Table 1 lists the values where that convergence approximately occurs as well as the values used in the actual study. Unfortunately, a 0.1% tolerance for all variables was far too computationally expensive. It order to manage this, tolerances for several variables were relaxed—these are italicized in the table. At these settings, each calculation required 512 cores so that the whole study (21 final configurations and testing) required up to 300,000 core hours—where each calculation was run out to 50 ms with a user-defined time step of 0.5 ms. The ALEGRA input script is provided in appendix C. Several scripts are also required to post-process the data: (appendix D) a shell script to automate generating text files of the inductances from simulations and (appendix E) MATLAB code to process and plot all of the data.

Table 1. Parameters and their convergence requirements.

Parameter to Converge	**Minimum Value Required for a 0.1% Tolerance**	**Actual Values Used**
Axial extent (multiples of coil length)	6	6
Azimuthal resolution (cells per $360°$)	120	120
Aztec tolerance	10^{-6}	10^{-6}
Mesh gap (inches)	*3*	*2*
Radial extent (multiples of outer conductor radii)	*4*	*3*
Radial mesh bias	12	12
Resolution (cells across conductor thickness)	*4*	*3*

Figure 2 illustrates some examples ($N_g = 2$ and 7, respectively) of the geometries to be evaluated for a 1/8-inch spacing between coils. Note the very long axial extent, which connect the coaxial section to the mesh boundary where current is supplied. This requirement is forced by boundary conditions but is not completely understood (see section B.2 for more details).

3. Inductance Scaling

Figure 3 plots the inductance as a function of time for several configurations with 1/4-inch air gap between the conductors. The magnetic diffusion time scale is on the order of tens of milliseconds—1 to 2 orders of magnitude larger than that for the coaxial cable. In each case, the

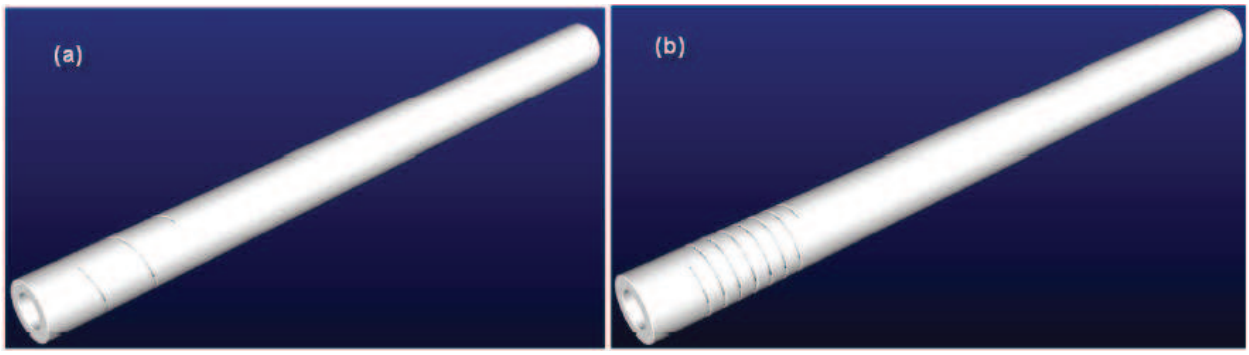

Figure 2. Helicoil with 1/8-inch air gap; and (a) $N_c = 1$, (b) $N_c = 6$.

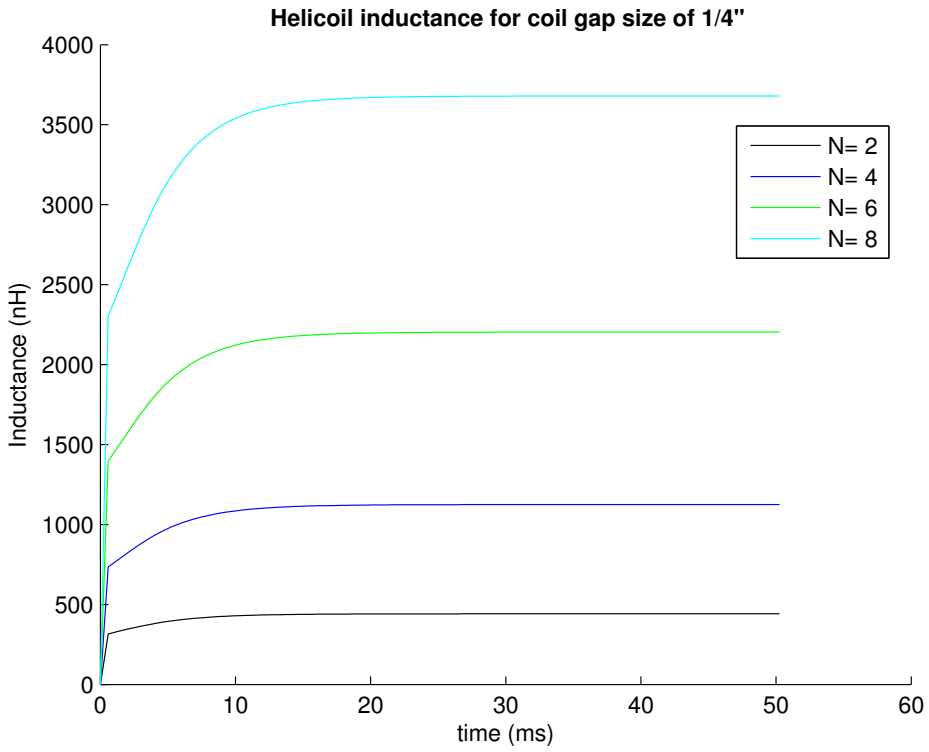

Figure 3. Helicoil inductances for a 1/4-inch air gap between the coils.

inductance starts to converge after about 10 ms. It is clear that the steady-state inductance is growing rapidly as the number of turns increases. Figure 4 displays the steady-state field for each coil configuration with a 1/4-inch air gap. In order to prevent color saturation at intermediate values of N_c, the color scale is biased so that its maximum values are based on $N_c = 9$. In each panel, horizontal bars represent the coaxial sections where the field between the inner and outer conductors dominate. It is apparent why certain convergence work is required. With more turns, a measurable amount of field couples to (or exceeds) the boundary. Consequently, that field is not tallied into the inductance leading to an erroneous result. Extent and magnitude of the fields

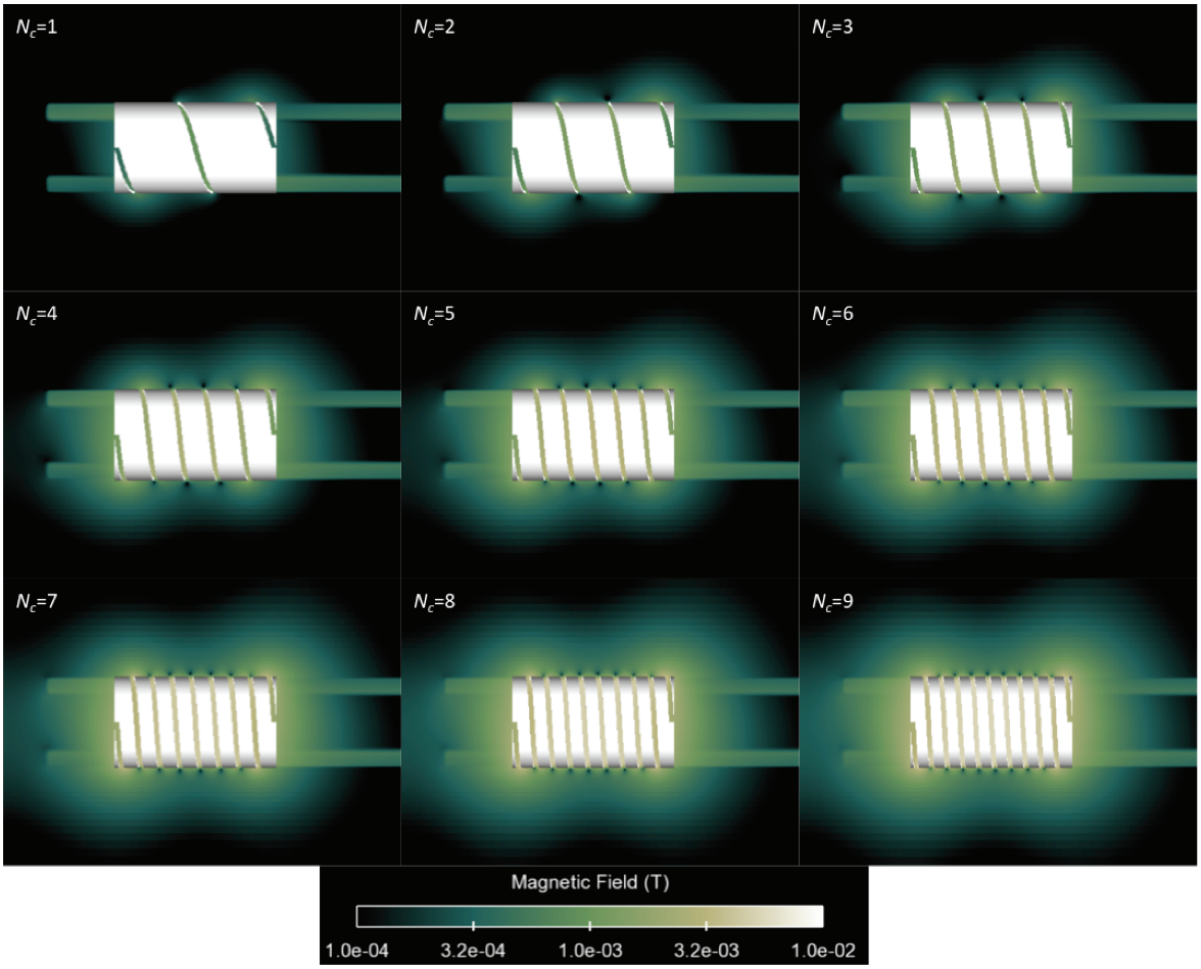

Figure 4. Helicoil geometries and their associated steady-state magnetic field distribution.

clearly grow with the number of turns—which is consistent with an increasing inductance as seen in equation 1. Appendix F illustrates these fields with coil visibility turned off

I encountered some difficulty in determining the most appropriate inductance to use from simulations, which was resolved by discussions with Satapathy (*18*), Bartkowski (*15*), and Berning (*1*). Specifically, we are interested in the self-inductance of an (hypothetical) isolated helicoil and interior conductor. The main question was whether subtracting off the coaxial inductance or that plus the additional energy to its radial exterior—due to the presence of the coil—was more appropriate. By subtracting off the analytic inductance, we are only considering the coaxial cable's self-inductance that is similar to Bartkowski and Berning's analysis. If I were to account for all energy from the boundary to the coil/coax transition, I would be subtracting off both self and only part of the mutual inductance between the coax and coil. The mutual inductance should be considered over all free space, which was not really possible to do here.

The series inductance from the adjacent coaxial sections can be determined analytically, and is evaluated to be 85 nH/m using equation A.12 with radial dimensions previously mentioned. The total coaxial contribution, 110 nH, is constant for all cases and subtracted from the inductance reported by ALEGRA so that figure 5 shows values for the coil section only. At large N, inductance due to the coaxial sections is very small; however, at small N, they are similarly-valued. As a comparison, an equivalently-sized device that is purely coaxial, has an inductance of 127.4 nH while ALEGRA determines it to be 126.8 nH, a 0.5% difference.

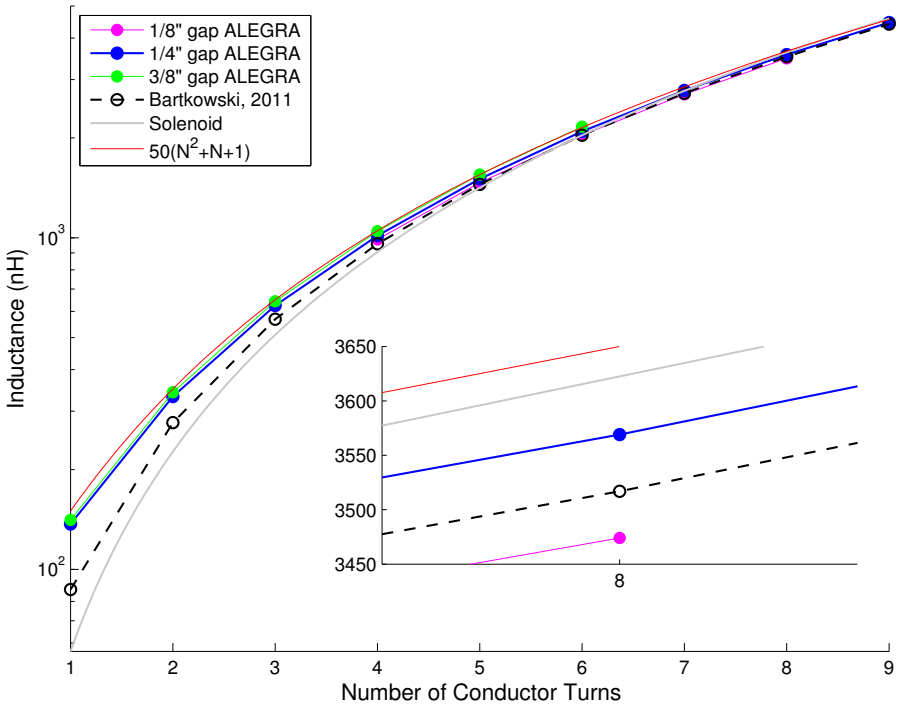

Figure 5. Helicoil inductance scaling.

Figure 5 illustrates the helicoil inductance scaling for several cases as well as data from Bartkowski and Berning (*9*). In that study they use a discrete-ring simplification in measuring coil inductance and numerical methods to evaluate the many elliptic integrals. It was expected however that the method would lose validity as N decreased. Niederhaus (*19*) suggested comparing the result from an equivalent solenoid,

$$L = \frac{\mu_0 \pi N^2 r_c^2}{z},$$

where r_c is the coil radius and z is the total coil length. I chose the radius to be the coil's inner surface as it had the best agreement with all other data series for large N. For the 1/4-inch geometry a surprisingly simple quadratic fit was found to be, $L[nH] = 50(N^2 + N + 1)$. In future work, I plan to build a model that incorporates the coil cross section—this should improve accuracy for inductance at small N.

All of the methods show remarkable agreement at large N. It was surprising though that the slot gap size had such a minor impact on the results. Those changes are on the order of our precision, which is constrained by computational cost. Satapathy (*18*) indicates that this lack of a gap size dependence could be due to the fact that the flux linkage remains the same for a given N. If we were to continue increasing N, eventually we would stop resolving the coils as more and more of them are squeezed over the same axial distance, decreasing the pitch and causing the helicoil to resemble a coaxial cable (since the air gaps would not be resolved). Consequently, inductance would drop—unphysically.

4. Conclusion

In this report, I have provided details on how inductance scales with the number of loops and gap size for helicoil inductors using ALEGRA. A great majority of the effort is spent ensuring proper convergence of relevant variables for an accurate solution, such as mesh size, resolution, grid biasing, and solver tolerance. Convergence was determined based upon an initial tolerance. If subsequent changes in the sensitive variables were less than the tolerance, then that variable had converged. Initially I chose 0.1% as the tolerance, however once all relevant variables were evaluated I discovered that production simulations had become too computationally expensive—each requiring thousands of cores for several hours. On our unclassified resources this was prohibitive given the tens of simulations required. Consequently, I backed off the tolerance on some of the variables, which brought the cost for each simulation down to about one thousand cores for several hours.

For these helicoil geometries, steady-state magnetic diffusion time requires several tens of milliseconds, up to two orders of magnitude greater than that required for coaxial conductors. Inductances are shown to scale quadratically with the number of conductor turns. At moderate to large N, results are in agreement with data provided by Bartkowski and Berning (*9*) as well inductance calculated for a simple solenoid—a function of the number of turns squared. It is clear then that as N increases, the squared term dominates so any linear or constant terms become

negligible. Errors will grow, however, with decreasing N. Interestingly, changes in the air gap between turns affect the solution by only a few percent so that the fit can be roughly applied to any gap size within the bounds investigated.

5. References

1. Berning, P. U.S. Army Research Laboratory, Aberdeen Proving Ground, MD. Private communication, May–June, 2012.

2. Jones, J. V. On the Calculation of the Coefficient of Mutual Induction of a Circle and a Coaxial Helix. *Proc. Phys. Soc. London* **1888**, *10*, 24.

3. Russell, A. The Magnetic Field and Inductance Coefficients of Circular, Cylindrical, and Helical Currents. *Philosophical Magazine and Journal of Science, XIII (6th series* **January–June 1907**, 420–446. January–June 1907.

4. Rosa, E. B.; Grover, F. W. Formulas and Tables for the Calculation of Mutual and Self-inductance (Revised). Scientific Papers of the Bureau of Standards. No. 169, 3rd Ed., Dec. 18, 1916.

5. Grover, F. W. *Inductance Calculations*; Dover Publications, Inc.: Mineola, NY, 1946.

6. Knoepfel, H. *Pulsed High Magnetic Fields*; North-Holland Publishing Company: Amsterdam, 1970.

7. Knoepfel, H. *Magnetic Fields*; John Wiley & Sons, Inc.: Toronto, Canada, 2000.

8. Turner, G. R. Turner Inductance Calculations For Helical Magnetocumulative Generators. *(Eur. J.) Electromagnetic Phenomena* **2003**, *3* (11), 392–396. http://emph.com.ua/ (accessed May 2013).

9. Bartkowski, P.; Berning, P. *Inductance Calculations of Variable Pitch Helical Inductors*; techanical report to be submitted for publication; U.S. Army Research Laboratory: Aberdeen Proving Ground, MD.

10. Niederhaus, J. H. *Verification for Simulating Magnetic Diffusion in a Simple Coaxial Cable*; techanical report to be submitted for publication; Sandia National Laboratories: Albuquerque, NM.

11. Jackson, J. D. *Classical Electrodynamics*; 3rd ed.; John Wiley & Sons, Inc.: New York, NY 1998.

12. Carroll, S. K. et al. *ALEGRA Users Manual*; Sandia National Laboratories: Albuquerque, NM, 2011.

13. Carroll, S. K. et al. *ALEGRA-MHD Users Manual*; Sandia National Laboratories: Albuquerque, NM, 2011.

14. Robinson, A.C . et al. *ALEGRA: An Arbitrary Lagrangian-Eulerian Multimaterial, Multiphysics Code*. 46th AIAA Aerospace Sciences Meeting and Exhibit, 2008-1235; Reno, NV, January 7–10, 2008.

15. Bartkowski, P. U.S. Army Research Laboratory, Aberdeen Proving Ground, MD. Personal Communication, May–June 2012.

16. Niederhaus, J. H. et al. ALEGRA Advanced/MHD Training Course (slide 99, session 4). Sandia National Laboratories: Albuquerque, NM, August 18–20, 2010.

17. Heroux, M. *AztecOO User Guide*; SAND2004-3796 (Revised); Sandia National Laboratories: Albuquerque, NM, August 2007. http://trilinos.sandia.gov/ (accessed May 2013).

18. Satapathy, S. U.S. Army Research Laboratory, Aberdeen Proving Ground, MD. Private communication, May–June, 2012.

19. Niederhaus, J. H. Sandia National Laboratories, Albuquerque, NM. Private communication, July 2012.

20. Robinson, A. Sandia National Laboratories, Albuquerque, NM. Unpublished work, April 2010.

Appendix A. Analytic Solution for the Inductance of a Coaxial Cable with Full-Field Diffusion

Equation 1 can be rewritten and broken into three regions representing the inner and outer conductors and the gap between them,

$$LI^2 = \mu \left(\int_{r_4}^{r_3} H_{43}^2 \, dV + \int_{r_3}^{r_2} H_{32}^2 \, dV + \int_{r_2}^{r_1} H_{21}^2 \, dV \right) \tag{A-1}$$

where $r_4 < r < r_3$ represents the inner conductor (region I), $r_3 < r < r_2$, represents the gap between conductors (region II), and $r_2 < r < r_1$ represents the outer conductor (region III). In order to proceed, the current density, J, in each region must also be evaluated which then provides a corresponding solution for H using the relation,

$$\oint \vec{H} \cdot \vec{dl} = \int \vec{J} \cdot \vec{ds}$$

where in cylindrical coordinates,

$$\begin{aligned} dl &= \rho \, d\phi = 2\pi\rho \\ ds &= \rho \, d\rho \, d\phi \end{aligned}$$

It should be noted that here, ρ, is a dummy radial variable and not material density.

In regions I and III, current density, $J = I/A$, is uniformly distributed through the conductors so that the enclosed current gives,

$$\begin{aligned} J_I &= \frac{I}{\pi(r_3^2 - r_4^2)} \\ J_{III} &= \frac{I}{\pi(r_1^2 - r_2^2)} \end{aligned}$$

In the gap, the enclosed current is simply I. Expressions for the magnetic field can now be evaluated giving,

$$H_I = \frac{I}{(2\pi r)\pi(r_3^2 - r_4^2)} \int_{r_4}^{r} \rho \, d\rho \int_0^{2\pi} d\phi = \frac{I(r^2 - r_4^2)}{2\pi r(r_3^2 - r_4^2)} \tag{A-2}$$

$$H_{II} = \frac{I}{2\pi r} \tag{A-3}$$

$$H_{III} = \frac{I}{(2\pi r)\pi(r_1^2 - r_2^2)} \int_{r}^{r_1} \rho \, d\rho \int_0^{2\pi} d\phi = \frac{I(r_1^2 - r^2)}{2\pi r(r_1^2 - r_2^2)} \tag{A-4}$$

Inserting equations A-2–A-4 into equation A-1 yields the following expression for the inductance,

$$LI^2 = \mu \left(\frac{I}{2\pi}\right)^2 \left\{ \int_{r_4}^{r_3} \frac{1}{r^2} \left(\frac{r^2 - r_4^2}{r_3^2 - r_4^2}\right) dV + \int_{r_3}^{r_2} \frac{dV}{r^2} + \int_{r_2}^{r_1} \frac{1}{r^2} \left(\frac{r_1^2 - r^2}{r_1^2 - r_2^2}\right) dV \right\} \tag{A-5}$$

Each of the integrals—I_1, I_2, and I_3, respectively—in equation A-5 can now be evaluated separately. Noting that in cylindrical coordinates, $dV = 2\pi l r \, dr$, and the r_i are constants,

$$\begin{aligned} I_1 &= \int_{r_4}^{r_3} \frac{2\pi l r}{r^2} \left(\frac{r^2 - r_4^2}{r_3^2 - r_4^2}\right)^2 dr = -\frac{2\pi l}{(r_3^2 - r_4^2)^2} \int_{r_4}^{r_3} \frac{1}{r}(r^4 - 2r^2 r_4^2 + r_4^4) \, dr \\ &= -\frac{2\pi l}{(r_4^2 - r_3^2)^2} \left\{ \frac{1}{4}(r_4^4 - r_3^4) - r_4^2(r_4^2 - r_3^2) + r_4^4 \ln\left(\frac{r_4}{r_3}\right) \right\} \end{aligned} \tag{A-6}$$

To put this and I_3 in a convenient form inspired by Robinson (*20*), equation A-6 needs to be rewritten. Assuming that $A = r_4$ and $B = r_3$, equation A-6 becomes,

$$-2\pi l \left\{ \frac{1}{4} \frac{(A^4 - B^4)}{(A^2 - B^2)^2} - A^2 \frac{(A^2 - B^2)}{(A^2 - B^2)^2} + A^4 \frac{\ln(A/B)}{(A^2 - B^2)^2} \right\} \tag{A-7}$$

but, $(A^4 - B^4) = (A - B)(A + B)(A^2 + B^2)$, so that

$$\frac{A^4 - B^4}{(A^2 - B^2)^2} = \frac{A^2 + B^2}{A^2 - B^2}$$

and equation A-7 becomes,

$$-2\pi l\left\{\frac{1}{4}\frac{(A^2+B^2)}{(A^2-B^2)}-\frac{A^2}{(A^2-B^2)}+\frac{A^4\ln(A/B)}{(A^2-B^2)^2}\right\} \tag{A-8}$$

Applying this to equation A-6 we obtain,

$$I_1=2\pi l\left\{-\frac{r_4^4\ln(r_4/r_3)}{(r_4^2-r_3^2)^2}+\frac{1}{4}\frac{(3r_4^2-r_3^2)}{(r_4^2-r_3^2)}\right\}. \tag{A-9}$$

When the same approach in equations A-7–A-8 is used to deal with quartic terms in I_3, one obtains,

$$I_3=2\pi l\left\{\frac{r_1^4\ln(r_1/r_2)}{(r_1^2-r_2^2)^2}-\frac{1}{4}\frac{(3r_1^2-r_2^2)}{(r_1^2-r_2^2)}\right\}. \tag{A-10}$$

Lastly, the solution to I_2 is easily obtained and results in,

$$I_2=2\pi l\ln\left(\frac{r_2}{r_3}\right). \tag{A-11}$$

Combining equations A-9–A-11 and inserting them into equqation A-5 yields the following expression for the inductance of a coaxial cable with uniform current density through the conductors,

$$L=\frac{\mu l}{2\pi}\left\{-\frac{r_4^4\ln(r_4/r_3)}{(r_4^2-r_3^2)^2}+\frac{1}{4}\frac{(3r_4^2-r_3^2)}{(r_4^2-r_3^2)}+\ln\left(\frac{r_2}{r_3}\right)+\frac{r_1^4\ln(r_1/r_2)}{(r_1^2-r_2^2)^2}-\frac{1}{4}\frac{(3r_1^2-r_2^2)}{(r_1^2-r_2^2)}\right\}. \tag{A-12}$$

INTENTIONALLY LEFT BLANK.

Appendix B. Mesh Convergence

There are a number of quantities that need to be evaluated for mesh convergence. This appendix provides the important details for determining what are the appropriate settings for variables relevant in ensuring an accurate solution. I monitored inductance, current, and resistance, however; this section only documents the former, which is the most useful. It is essential to pick the most constraining cases to test for convergence or else results from more constraining answers can give inaccurate results. Figure B-1 illustrates this for the 1/8-inch case for small N—originally I assumed that large N would be the more constraining case. For this study we are interested in converging inductance to the point where the fractional change no more than 1%. In most cases, each convergence property is only compared against iterations of itself. Few combinatorial cases are considered. Originally, the goal was to have a 0.1% constraint, but that had to be relaxed due to the significant computational cost in asserting such a tolerance.

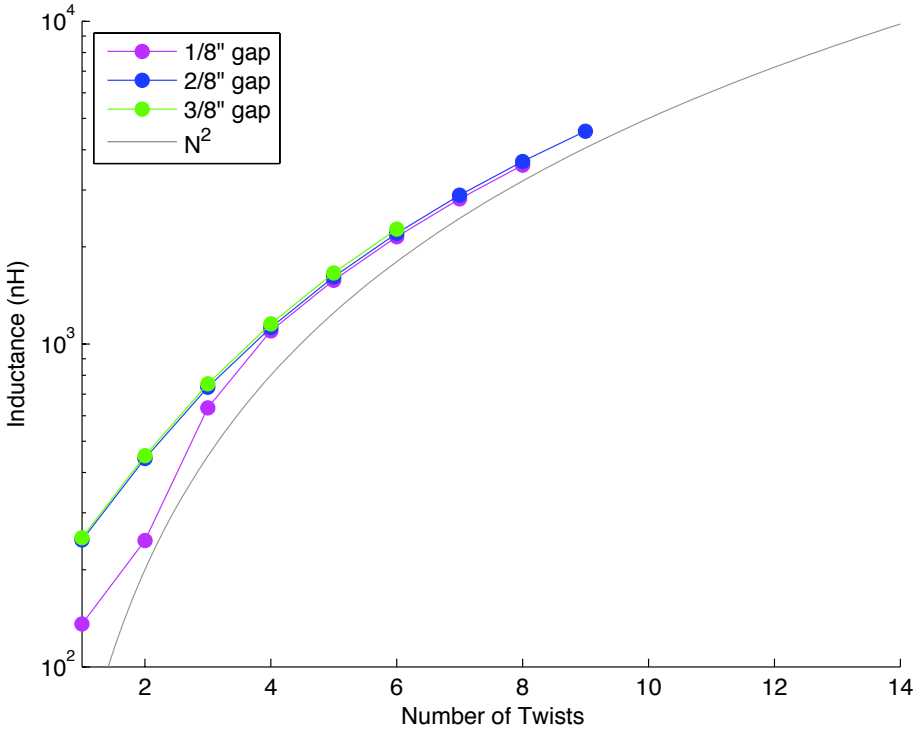

Figure B-1. Inductance trends illustrating results that are not appropriately converged (1/8-in air gap, small N).

B.1 Resolution

Resolution is a common metric for convergence since the smallest object of interest must be resolved. Because it controls the total number of cells in a simulation, it strongly affects total calculation time. In our case that feature is usually either the spacing between loops or the thickness of the conductors, whichever is smaller. If the air gaps between loops in the helix are not resolved, the structure is lost and simply appears as a continuous (coaxial) conductor which has an inductance several orders of magnitude lower than a helicoil. For our cylindrical mesh, the radial, axial, and azimuthal resolution must be evaluated.

Figure B-2 illustrates the inductance and its fractional change as a function of the number cells across the conductor thickness when the air gap is 1/4 in. Recall that this is evaluated for the thinnest conductor which is 1/8 in thick. These results indicate that we should have at least about four cells across the conductor for a tolerance of 0.1%. Due to computational cost, this requirement was relaxed to three.

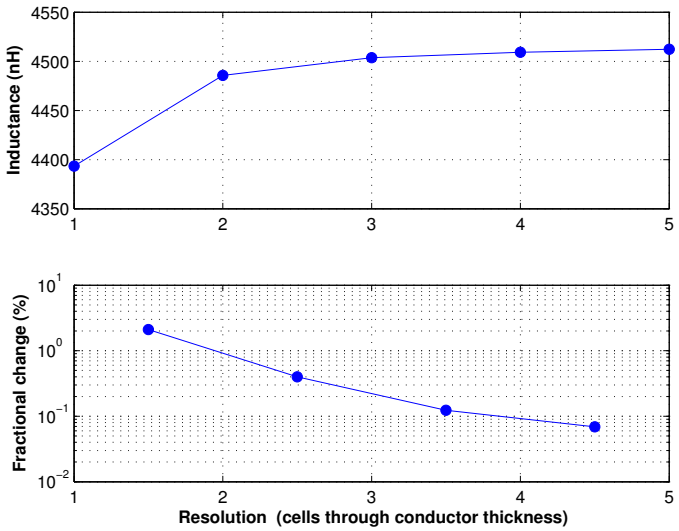

Figure B-2. Inductance and its fractional change as a function of the number of cells through the conductor thickness for a 1/4-in air gap between the coils.

Figure B-3 illustrates the inductance and its fractional change as a function of the number cells across the conductor thickness when the air gap is 1/8 in. These results also conclude that at least 4 cells are required. Note the massive jump in inductance when transitioning from 2 to 3 cells across the conductor. At low resolutions, two cells still cannot resolve the coils so the structure appears continuous, resembling coaxial cable.

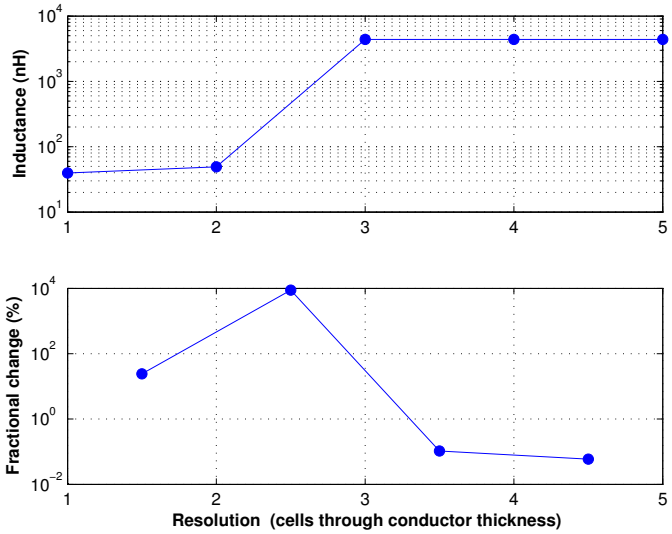

Figure B-3. Inductance and its fractional change as a function of the number of cells through the conductor thickness for a 1/8-in air gap between the coils.

Figure B-4 illustrates the current and its fractional change as a function of the number of azimuthal cells comprising the 360 degrees extent of the mesh. The data indicates that in going from 80 to 120 cells, there is an approximate 0.15% change in the current. From 200 to 240 cells, that change drops to 0.01%. Current converges to our threshold once we have at least 120 azimuthal cells.

Figure B-5 repeats these comparisons, but for inductance. The data shows that there is a 0.2% change in going from 80 to 120 cells about the mesh while that drops to 0.1% in going from 120 to 160 cells. The inductance, rather than current, is the driving constraint for azimuthal resolution. We therefore select a minimum of 160 cells as our azimuthal resolution.

B.2 Mesh Size

The inductance, L, is calculated from the magnetic energy, E_m, as, $L = 2E_m/I^2$, where I is the current. Recalling equation 1, we can see that that the inductance is directly coupled to the amount of magnetic field in the computational domain. Thus if the volume or mesh is not large enough, an insufficient amount of field will be tallied leading to an incorrect inductance. Both the axial and radial extent therefore need to be evaluated for convergence.

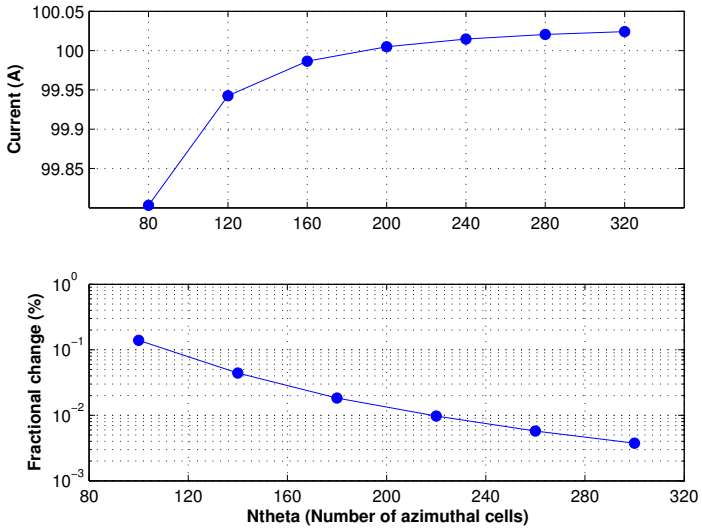

Figure B-4. Current and its fractional change as a function of the number of azimuthal cells.

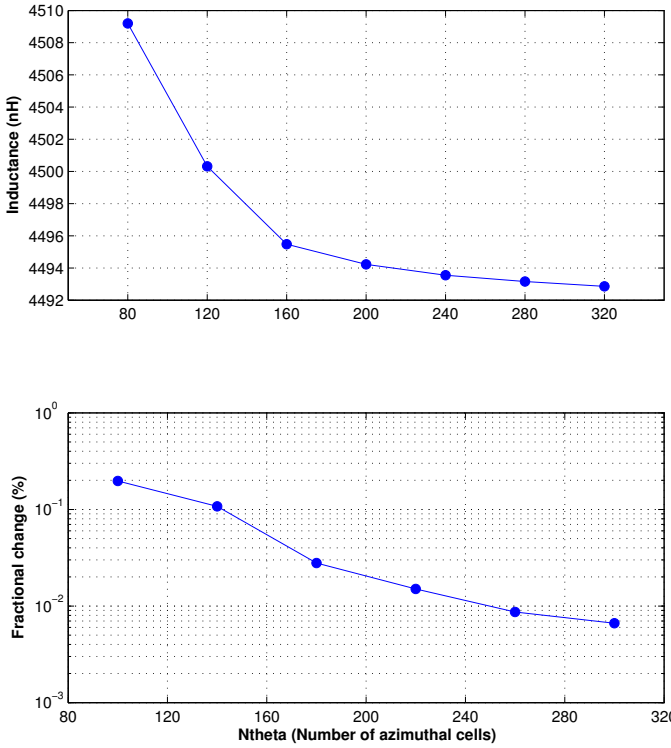

Figure B-5. Inductance and its fractional change as a function of the number of azimuthal cells.

Radially, the inductance is illustrated in figure B-6 in multiples of the outer conductor's outer radius. We find that a radial extent of 3 radii is sufficient to meet our convergence tolerance. Current is not illustrated as all values of the outer conductor radii already yielded acceptable results. Curiously, in figure B-6 as well as figure B-7, even though the amount of mesh is increasing, the inductance is actually going down. This is counter-intuitive and not yet understood completely. At the time of publication, the variable `EPOYNT` is found to be changing with mesh size. This quantity represents the total electromagnetic energy being dumped into the domain, which should be independent of mesh size [Ni2012].

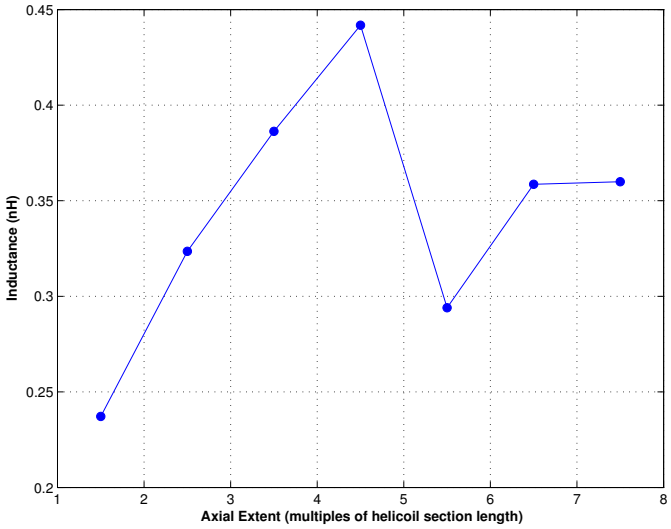

Figure B-6. Inductance for axial extent.

In order to satisfy magnetic field boundary conditions, the coil needs to be sufficiently far from the boundary where current enters the mesh. This can be accomplished by inserting a long coaxial section between the coil and boundary. However this adds inductance (given by equation A-12) which is directly proportional to the coaxial length. Specifically, that amount is 17.2 nH for an 8-in coaxial length (our coil length). Nominally, inductance in the simulations should only increase by this much as well. However, there will be variations due to non-convergence for some variables as well as general convergence as more field is captured with an increasingly distant axial boundary. Figure B-6 illustrates this behavior where the difference between increasingly larger coaxial sections is compared with the analytic value. The plot indicates that it takes an additional coaxial section of at least six coil lengths (4 feet) before results begin to converge. This is one of the biggest computational costs and is driving development of a new capability in Alegra referred to as "potential drive" where the user specifies an electric potential

across the mesh [Ni2012]. Additionally some of this cost could be relaxed by introducing an axially biased mesh in the added coaxial section, but this was not performed. A final component of the axial study is the gap between the non-current supplying mesh boundary and end cap of the device. Convergence of this "mesh gap" is illustrated in figure B-7. The data shows that three inches are required to satisfy our convergence tolerance.

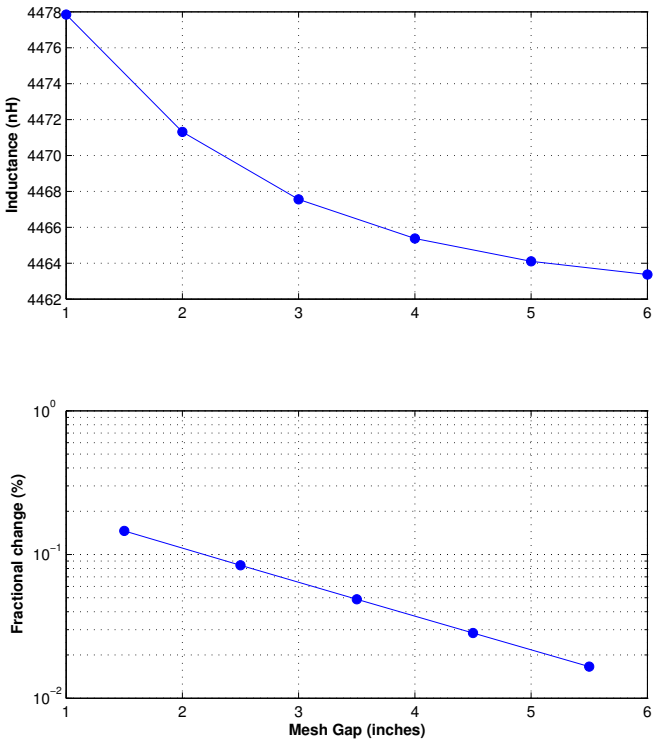

Figure B-7. Inductance and its fractional change as a function of the mesh gap.

B.3 Radial Mesh Bias

Because these studies may require the mesh to grow quite large, it is useful to look for ways to reduce the total number of elements to keep total simulation time down. This would be useful where there are only field quantities, such as those radially distant from the conductors. We can apply a mesh bias such that the resolution decreases as we move further away from the outer conductor. This quantity should also be checked such that resolution does not become so coarse as to affect the inductance. For all cases of the mesh coarsening multiplier (2-12x), we found that results did not change more than our convergence threshold (figure B-8).

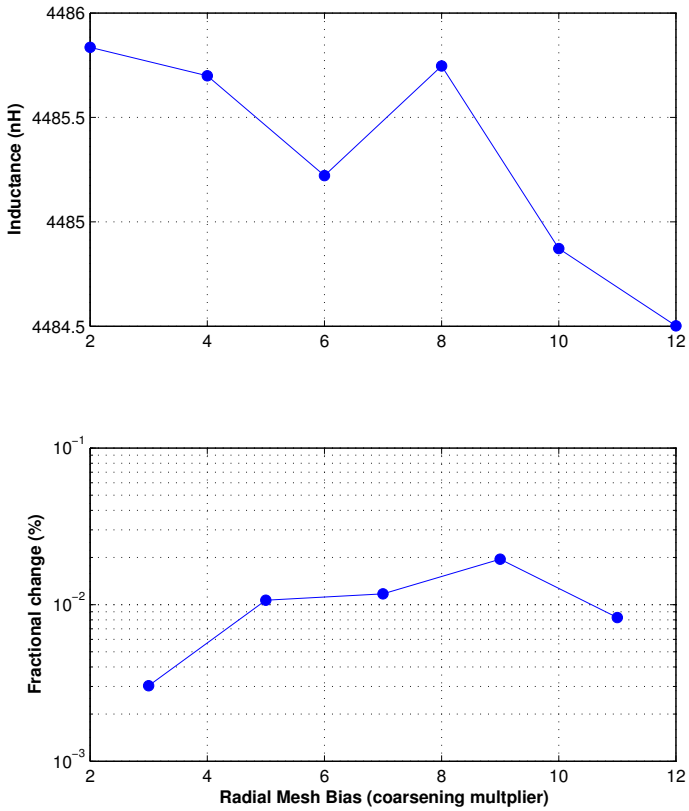

Figure B-8. Inductance and its fractional change as a function of radial mesh biasing.

B.4 Solver Tolerance

Finally, during the simulation the magnetic solver, AztecOO [He2007], iterates towards a solution every cycle. A user-defined threshold indicates the amount of accuracy in determining whether it needs to iterate further or whether it has achieved a solution for that cycle. This Aztec tolerance also needs to be evaluated for convergence. If the tolerance is too loose, wildly inaccurate answers can result. On the other hand, a tolerance too tight can give you the correct answer but take an inordinate amount of time due to the increased precision. As figure B-9 indicates, changing the tolerance from 10^{-4} to 10^{-6} can reduce the inductance about 1%. Tolerances tighter than that have little effect on the results. Consequently, I chose 10^{-6} for this study.

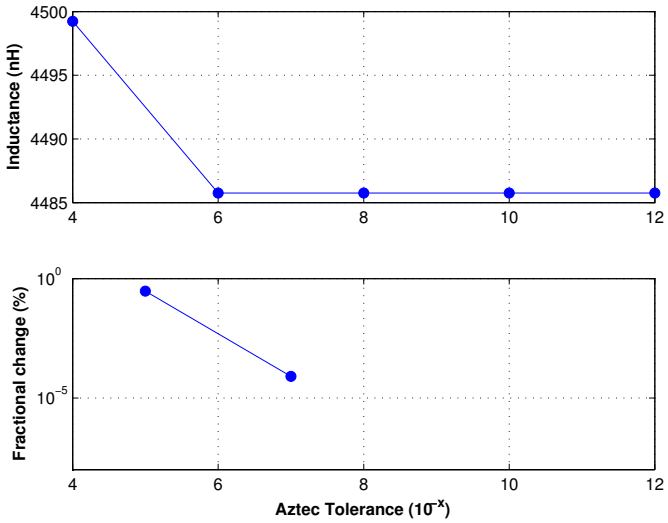

Figure B-9. Inductance and its fractional change as a function of the magnetic solver.

Appendix C. Sample Input Script for Alegra Calculations Using Dakota

```
$---------------------------------
$
$ Helicoil
$
$ R. Doney
$ Oct. 2011
$
$---------------------------------

${_FORMAT="%.10g"}
${in2m = 0.0254}

$ --- Dakota ---
$ dakota comments use #

dakota input = "
strategy,
        single_method
        tabular_graphics_data
        tabular_graphics_file = 'opt_history_data'

interface,
        direct
          analysis_driver = 'alegra'
          processors_per_analysis = 512
# asynchronous

variables,
        continuous_design = 1
         lower_bounds 1
         upper_bounds 9
         descriptors '_NumCondTwists_'

responses,
        num_objective_functions = 1
        no_gradients
        no_hessians

method,
        multidim_parameter_study
        partitions 8
"
end


$dt:{dt = 500.0e-6} $ Set time manually
$TermTime:{TermTime = 50.0e-3} $ End simulation (s)
$NumCycles:{NumCycles = TermTime/dt} $ Number of cycles
```

```
$ --- Resolution setting ---
$MagDiffRes:{MagDiffRes = 3}
$SlotWidthRes:{SlotWidthRes = 2} $ Number of elements across gap between conductor twists


$ --- Inner Conductor ---
$arm_thick:{arm_thick = 1/4*in2m}
$d_arm_out:{d_arm_out = 3*in2m}
$r_arm_out:{r_arm_out = d_arm_out/2}
$r_arm_in: {r_arm_in = r_arm_out-arm_thick}
$r_arm_center:{r_arm_center = (r_arm_in+r_arm_out)/2}
$plate_thick:{plate_thick = 1/4*in2m}


$ --- Outer Conductor ---
$helix_thick:{helix_thick = 1/8*in2m}
$d_helix_out:{d_helix_out = 4.5*in2m}
$r_helix_out:{r_helix_out = d_helix_out/2}
$r_helix_in: {r_helix_in = r_helix_out-helix_thick}
$r_helix_center:{r_helix_center = (r_helix_in + r_helix_out)/2}


$ --- Helix characteristics ---
$ The simulational current feed length needs to be a multiple of the total helical length

$Helix2BndryMultiplier:{Helix2BndryMultiplier = 6}
${Lmiddle = 8*in2m} $ length of helical section (m)
${Ltail   = 3.25*in2m} $ Length of outer conductor tail (m)
${Lfeed   = Helix2BndryMultiplier*Lmiddle} $ Length of simulational current feed (m)
${LfeedE  = 3.5*in2m} $ Length of experimental current feed (m)
${L    = Lfeed + Ltail + Lmiddle} $ Conductor length excluding cap (m)
${Linches = L/in2m} $ Conductor length excluding cap (inches)

${slotwidth = 1/4*in2m}
${NumGapTwists = _NumCondTwists_+1} $ Number of slot (gap) twists
${pitch   = (Lmiddle-slotwidth)/NumGapTwists} $ Pitch (m/turn)
${pitchIn = pitch/in2m} $ Pitch (inches/turn)


$ --- Mesh Size ---
$r_field:{r_field = 3*r_helix_out} $ Amount of mesh to include beyond outer conductor (m)
$r_mesh: {r_mesh = r_helix_out + r_field} $ Max radial extent of mesh
$MeshGap:{MeshGap = 2.0*in2m} $ Mesh padding between boundary and cap
$RadBias:{RadBias = 12} $ Radially bias the mesh to make coarser

$ --- Calculate Magnetic Diffusion Time ---
$CurrentRampTime:{CurrentRampTime = 5.0e-6}
$ConstEcon:{ConstEcon = 1.0e6}
$ConstEcon:{ConstEcon = 2.5e7}
$MaxCondThick:{MaxCondThick=max(arm_thick,helix_thick)}
$MagDiffTime:{MagDiffTime = 1.0e6 * ConstEcon * 4*PI*1.0e-7 * MaxCondThick^2} $ microseconds


$ --- Determine resolution ---
$SIZE1:{SIZE1 = slotwidth/SlotWidthRes} $ Resolve based on Air gap between loops
```

```
$SIZE2:{SIZE2 = helix_thick/MagDiffRes} $ Resolve based on conductor thickness
$CELL_SIZE:{CELL_SIZE = min(SIZE1,SIZE2)}

$ 1.05 is used to fix truncation to 0 errors from using 'int'
$arm_cell_size:{arm_cell_size = arm_thick/int(arm_thick/CELL_SIZE+1.05)}

${angle = 360}
${ntheta = 120}

${GMIN_X = 0}
${GMIN_Y = 0}
${GMIN_Z = 0}
${GMAX_X = r_mesh}
${GMAX_Y = angle}
${GMAX_Z = L+plate_thick+MeshGap}


$ ------------------------------------------------------------------------

title: Constant pitch helicoil
units, si

termination time {TermTime}
$termination cycle 1

transient magnetics

 void conductivity, 1.0e-3
 delta time {dt}

 response functions
    tracer 100, variable = COORDINATES, Y, end
 end

$ --- Define mesh
${NumZ = 1}
${NumR = 5}
${NumA = 1}
mesh, inline
   radial trisection
trisection blocks, 4
transition radius, {0.5*r_arm_in}

   numz {NumZ}
zblock 1 {GMAX_Z} first size {CELL_SIZE}

   numr {NumR}
rblock 1 {r_arm_in} first size {arm_cell_size}
rblock 2 {r_arm_out - r_arm_in} interval {MagDiffRes}
rblock 3 {r_helix_in - r_arm_out} first size {CELL_SIZE}
rblock 4 {r_helix_out - r_helix_in} interval {MagDiffRes}
rblock 5 {r_mesh - r_helix_out} first size {CELL_SIZE} last size {RadBias*CELL_SIZE}

   numa {NumA}
ablock 1 {angle} interval {int(ntheta)}
```

```
   end

   set assign
nodeset, ihi, 20 $ r high
nodeset, jhi, 30 $ theta high
nodeset, jlo, 40 $ theta low
nodeset, khi, 50 $ z high
nodeset, klo, 60 $ z low (current feed)
sideset, ihi, 20
        sideset, jhi, 30
        sideset, jlo, 40
        sideset, khi, 50
        sideset, klo, 60
   end
end

tracer points
  eulerian tracer 100 x {r_arm_center} y 0 z {Lfeed}
end


block 1 to {NumR * NumZ * NumA}
eulerian mesh
add diatom input
end


$ --- TRANSIENT MAGNETICS ---
current tally, 1, sideset 60, end

cylindrical axial slot bc, sideset 60, 100.0, EXCLUDE MATERIAL 1,
x 0. y 0. z 0.
x 0. y 0. z {GMAX_Z}
{r_arm_center},{r_arm_center},{r_helix_center},{r_helix_center}

$   circuit node 1 fixedv 0.0
$   circuit node 2
$   circuit node 3
$   circuit node 4 startv -10.0e3

$   circuit element, 1 2, mesh
$   circuit element, 2 3, resistor, 1.0e-3
$   circuit element, 3 4, inductor, 215.0e-9
$   circuit element, 4 1, capacitor, 525.0e-6

$   circuit solver, rel 1.0e-5, abs 1.0e-2

   e tangent bc, sideset 60, 0.0, MATERIAL 1, x 0.0 y 1.0 z 1.0

   aztec set, 1



diom insertion algorithm, hex
```

```
diatom

package InnerConductor
  material 1
  numsub 50
  insert cylinder
ce1 0 0 {GMIN_Z}
ce2  0 0 {L}
rinner {r_arm_in}
radius {r_arm_out}
  endinsert
endpackage


package OuterConductorFeed
  material 1
  numsub 50
  insert cylinder
        ce1     0 0 {GMIN_Z}
        ce2     0 0 {Lfeed}
        rinner  {r_helix_in}
        radius  {r_helix_out}
  endinsert
endpackage


package OuterConductorTail
  material 1
  numsub 50
  insert cylinder
        ce1     0 0 {L-Ltail}
        ce2     0 0 {L}
        rinner  {r_helix_in}
        radius  {r_helix_out}
  endinsert
endpackage


package ReturnDisk
  material 1
  numsub 50
  insert cylinder
        ce1     0 0 {L}
        ce2     0 0 {L+plate_thick}
        rinner  {r_arm_in}
        radius  {r_helix_out}
  endinsert
endpackage


package 'Helix middle section'
  material 2
  numsub 50
  insert cylinder
```

```
        ce1     0 0 {Lfeed}
        ce2     0 0 {Lfeed + Lmiddle}
        rinner  {r_helix_in}
        radius  {r_helix_out}
  endinsert
  delete r2dp
ce1 = 0.0 0.0 {Lfeed}
ce2 = 0.0 0.0 {Lfeed + Lmiddle}

$ These points are in (u,v) space which is defined by CE1 and CE2
$ Here we use (r,z)
$ dr: {dr = 0.5*helix_thick}
$ Need dr because without it, current can still flow across gap

p = {r_helix_in - dr} 0
p = {r_helix_out + dr} 0
p = {r_helix_out + dr} {slotwidth}
p = {r_helix_in - dr} {slotwidth}

ce3 = 0.0 1.0 0.0 $ direction of rotation for helix
pitch = 0.0 {pitch} $ (u,v) space
twist = {NumGapTwists}
  enddelete
endpackage

enddiatom


end $ End Physics -------------------------------------


aztec 1
  solver, cg
  scaling, none
  conv norm, rhs
  max iter, 10000
  tol = 1.0e-8

  multilevel
   fine sweeps = 1
   fine smoother = Hiptmair
   coarse smoother = LU
   multigrid levels = 10
   interpolation algorithm = AGGREGATION
   smooth prolongator
  end
end

$ --- Plot details ---
emit output: time = {dt}
emit hisplt: time interval = {dt}
emit plot: time interval = {dt}

Plot variable
  je
```

```
  be
  density
  density, avg
  scalar conductivity
end


$ --- Materials ---

material 1 Aluminum
  model = 100 $ CTH EP
  model = 105 $ Econ
end

model 100, keos miegruneisen
  matlabel = '6061-T6_AL'
end

model 105, ec knoepfel
  sigma0 = {ConstEcon}
  alpha = 0.0
  betacv = 0.0
end


$ ------------------

material 2 Aluminum
  model = 100
  model = 105
end

exit
```

INTENTIONALLY LEFT BLANK.

Appendix D. Example Shiv Script for Batch Processing

To extract the relevant data out of .his files generated by ALEGRA, one can script "shiv" for batch processing. This script may be run from the UNIX command line.

```
#!/bin/csh -f

set TMPD = /Users/rdoney/MFC/InductanceStudy/Ntheta
cd $TMPD
set INPUT = CoilN9s14r4t
set RunID = 120
while ($RunID <= 320)
  set FILENAME = ${INPUT}${RunID}
  printf "Processing ${FILENAME}...\n"
  mkdir ${FILENAME}TxtFiles
  shiv -b -g CURRENT "./${FILENAME}.his" > "${FILENAME}TxtFiles/${FILENAME}_CURRENT.txt"
  shiv -b -g INDUCTANCE "./${FILENAME}.his" > "${FILENAME}TxtFiles/${FILENAME}_INDUCTANCE.txt"
  shiv -b -g RESISTANCE "./${FILENAME}.his" > "${FILENAME}TxtFiles/${FILENAME}_RESISTANCE.txt"
  shiv -b -g GRINDNOIO "./${FILENAME}.his" > "${FILENAME}TxtFiles/${FILENAME}_GRINDNOIO.txt"
  @ RunID = ${RunID} + 40
end
```

INTENTIONALLY LEFT BLANK.

Appendix E. MATLAB Script for Post-processing

```
%% INDUCTANCE CONVERGENCE STUDY
% Bobby Doney
% 1 Sep. 2011
% 2 Feb. 2012: Need to still update automation of axial extent. Pieces are
% there, but it's not based on selecting it as the 'study' variable

in2m = 0.0254;
in2mm = in2m*1e3;

%% Establish which study we are looking at and setup up values unique to that case

% Study name must match data directory names, but with whitespace.
%study = 'Axial Extent'
study = 'Aztec Tolerance'
%study = 'Mesh Gap'
%study = 'Ntheta'
%study = 'Radial Extent'
%study = 'Radial Mesh Bias';
%study = 'Resolution';

res = 'QuarterInch';
%res = 'EighthInch';

% Variable: Convert relevant variable name to displayable form
VARIABLE = 'INDUCTANCE';
%VARIABLE = 'CURRENT';
%VARIABLE = 'RESISTANCE';
%VARIABLE = 'GRINDNOIO';

variable = lower(VARIABLE);
Variable = regexprep(variable,'(\<[a-z])','${upper($1)}');

% Remove whitespaces from study name to match directory names
studyNoWS = regexprep(study,'[^\w'']','');

% Make custom filename for saved EPS image
printfilename = [studyNoWS,Variable];


switch study
    case 'Axial Extent'
        nameprefix = 'CoilN9s14r2Ax';
        IDstart = 1;
        IDstep = 1;
        IDend = 8;
        XLabelName = ['\bf',study,' (multiples of helicoil section length)'];
    case 'Aztec Tolerance'
        nameprefix = 'CoilTol_e-';
```

```
        IDstart = 4;
        IDstep = 2;
        IDend = 12;
        XLabelName = ['\bf',study,' (10^{-x})'];
    case 'Mesh Gap'
        nameprefix = 'CoilN9s14Gap';
        IDstart = 1;
        IDstep = 1;
        IDend = 6;
        XLabelName = ['\bf',study,' (inches)'];
    case 'Ntheta'
        nameprefix = 'CoilN9s14r4t';
        IDstart = 80;
        IDstep = 40;
        IDend = 320;
        XLabelName = ['\bf',study,' (Number of azimuthal cells)'];
    case 'Radial Extent'
        nameprefix = 'CoilN9s14r2R';
        IDstart = 1;
        IDstep = 1;
        IDend = 4;
        XLabelName = ['\bf',study,' (multiples of outer conductor radii)'];
    case 'Radial Mesh Bias'
        nameprefix = 'R3RadMeshBias';
        IDstart = 2;
        IDstep = 2;
        IDend = 12;
        XLabelName = ['\bf',study,' (coarsening multplier)'];
    case 'Resolution'
        switch res
            case 'EighthInch'
                nameprefix = 'CoilN9s18r';
                printfilename = [studyNoWS,Variable,'s18'];
            case 'QuarterInch'
                nameprefix = 'CoilN9s14r';
                printfilename = [studyNoWS,Variable,'s14'];
            otherwise
                disp('Resolution Name is incorrect');
                quit cancel
        end
        IDstart = 1;
        IDstep = 1;
        IDend = 5;
        XLabelName = ['\bf',study,'  (cells through conductor thickness)'];
end


format compact
source_dir = ['/Users/rdoney/Research/MFC/InductanceStudy/',studyNoWS];
cd (source_dir);


i=1;    % initialize results vector index

%% Read in all of the data from the txt files generated by shiv
```

```
for EvalID = IDstart:IDstep:IDend
    % Build up the directory and file name of the current evaluation
    CurrentEvalName = ([nameprefix,num2str(EvalID)]);

    % Check to see if relevant data exists
    if exist([CurrentEvalName,'TxtFiles'],'dir')
        disp([pwd,'/',CurrentEvalName,' exists'])
        % Read in the data for the current Dakota evaluation.
        % Each file has time as the first column and some other VARIABLE as the
        % second.
        xyDataFileImport([CurrentEvalName,'TxtFiles/',CurrentEvalName,'_',VARIABLE,'.txt'])

    % Some datasets use an original baseline rather than rerunning that sim
    % over again. There are only 2 cases of that. We need to use those .his
    % files to fill in the missing data. There are only 2 baseline
    % refs, and only 1 case of one of those. That data will have to be
    % read in and processed just like above.
    else
        BaselineDir = '/Users/rdoney/Research/MFC/InductanceStudy/Resolution';
        switch studyNoWS
            case 'Ntheta'
                BaselineFile = 'CoilN9s14r4';
            otherwise
                BaselineFile = 'CoilN9s14r2';
        end
        disp([CurrentEvalName,' does not exist, using ',BaselineFile])
        xyDataFileImport([BaselineDir,'/',BaselineFile,'TxtFiles/',BaselineFile,'_',VARIABLE,'.txt'])
    end

    %Store the time for each evaluation as a column in the TIME matrix
    TIME(:,EvalID) = data(:,1)*1e3;         % milliseconds

    %Store the VarTimeSeries for each evaluation as a column in the VarTimeSeries matrix
    switch VARIABLE
        case 'INDUCTANCE'
            VarTimeSeries(:,EvalID) = data(:,2)*1e9;    % nanohenries
        case 'CURRENT'
            VarTimeSeries(:,EvalID) = data(:,2);        % amps
        case 'RESISTANCE'
            VarTimeSeries(:,EvalID) = data(:,2)*1e3;    % milliohms
        case 'GRINDNOIO'
            VarTimeSeries(:,EvalID) = data(:,2)*1e6;    % microseconds
    end

    % Grab the last data point for each evaluation - which should be the
    % converged value
    ConvergenceVar(i) =  VarTimeSeries( length(VarTimeSeries(:,1)) , EvalID);

    i=i+1;
end

%% Calculate analytic inductance per unit length using dimensions from sims

% Inner Conductor
arm_thick = 1/4*in2m;
```

```
d_arm_out = 3*in2m;
r_arm_out = d_arm_out/2;
r_arm_in = r_arm_out-arm_thick;
r_arm_center = (r_arm_in+r_arm_out)/2;

% Outer Conductor
helix_thick = 1/8*in2m;
d_helix_out = 4.5*in2m;
r_helix_out = d_helix_out/2;
r_helix_in = r_helix_out-helix_thick;
r_helix_center = (r_helix_in + r_helix_out)/2;


Lmiddle= 8*in2m;
Lback  = 3.25*in2m;         % length of current return (m)
Lfront = Lmiddle*[1:1:8];   % length of current feed (Multiples of Lmiddle) (m)
h      = Lfront + Lback;    % Total length of coaxial pieces (m)


% Using NiederhausÕ notation
mu = 4*pi*1e-7;

r4 = r_arm_in;
r3 = r_arm_out;
r2 = r_helix_in;
r1 = r_helix_out;
e3 = -(r4^4*log(r4/r3))/(r4^2-r3^2)^2 + 0.25*(3*r4^2-r3^2)/(r4^2-r3^2);
e2 = log(r2/r3);
e1 = (r1^4*log(r1/r2))/(r1^2-r2^2)^2 - 0.25*(3*r1^2-r2^2)/(r1^2-r2^2);

L3 = mu/(2*pi)*e3;  % Inductance per unit length
L2 = mu/(2*pi)*e2;  % Inductance per unit length
L1 = mu/(2*pi)*e1;  % Inductance per unit length

LperLengthAnalytic_nH_m  = 1e9*(L1+L2+L3);  % Inductance per unit length (nH/m)

L_nH = LperLengthAnalytic_nH_m*Lfront;       % Analytic Inductance for different coax lengths (nH)



% If we subtract off the growth in inductance due to the increasing feed
% length, the total inductance should remain approximately the same since
% nothing else is changing.

% analytic coaxial inductance for 1 coil length = 17.2024 nH

% AxialConv = ConvergenceVar - L_nH;
% for i=1:length(ConvergenceVar)-1
%     dConvergenceVar(i) = abs(AxialConv(i+1) - AxialConv(i));
% end

%set(gca,'XTickLabel',{'1';'2';'3';'4';'5';'6';'7';'8';'9'})

%% Plot data
```

```
switch VARIABLE
    case 'INDUCTANCE'
        YLabelName = ['\bf',Variable,' (nH)'];
    case 'CURRENT'
        YLabelName = ['\bf',Variable,' (A)'];
    case 'RESISTANCE'
        YLabelName = ['\bf',Variable,' (m\Omega)'];
    case 'GRINDNOIO'
        YLabelName = ['\bf',Variable,' (\mus)'];
end

% Axial Length Case

% plot(1.5:1:7.5,dConvergenceVar,'-ob','MarkerFaceColor','Blue')
% ylabel(YLabelName)
% grid
% set(gca,'Box','on')
% xlabel(XLabelName)


h=figure;
subplot(2,1,1)
plot(IDstart:IDstep:IDend,ConvergenceVar,'bo-','MarkerFaceColor','blue')
%plot(IDstart:IDstep:IDend,ConvergenceVar./Lfront,'bo-','MarkerFaceColor','blue')
%plot(IDstart:IDstep:IDend,dConvergenceVar,'bo-','MarkerFaceColor','blue')
ylabel(YLabelName)
grid
set(gca,'XTick',IDstart:IDstep:IDend,'Box','on')
%print(h,'-depsc',[printfilename,'.eps'])

%
% Fractional change in the results
NewConvergenceVar = ConvergenceVar;
%NewConvergenceVar = ConvergenceVar./Lfront;

for i=2:length(NewConvergenceVar)
    FracChng(i-1) = abs( ( NewConvergenceVar(i) - NewConvergenceVar(i-1) )/NewConvergenceVar(i-1) ) *100;
end
XaxesStart  = mean([IDstart:IDstart+IDstep])
XaxesEnd    = mean([IDend-IDstep:IDend])

subplot(2,1,2)
plot(XaxesStart:IDstep:XaxesEnd,FracChng,'o-','MarkerFaceColor','blue')
set(gca,'YScale','log')
YaxisLimits = get(gca,'YLim');
axis([IDstart IDend YaxisLimits(1) YaxisLimits(2)])
grid
xlabel(XLabelName)
ylabel('\bfFractional change (%)')
set(gca,'XTick',IDstart:IDstep:IDend,'Box','on')
```

INTENTIONALLY LEFT BLANK.

Appendix F. Magnetic Field Behavior Without Coil (As Compared to Figure 6)

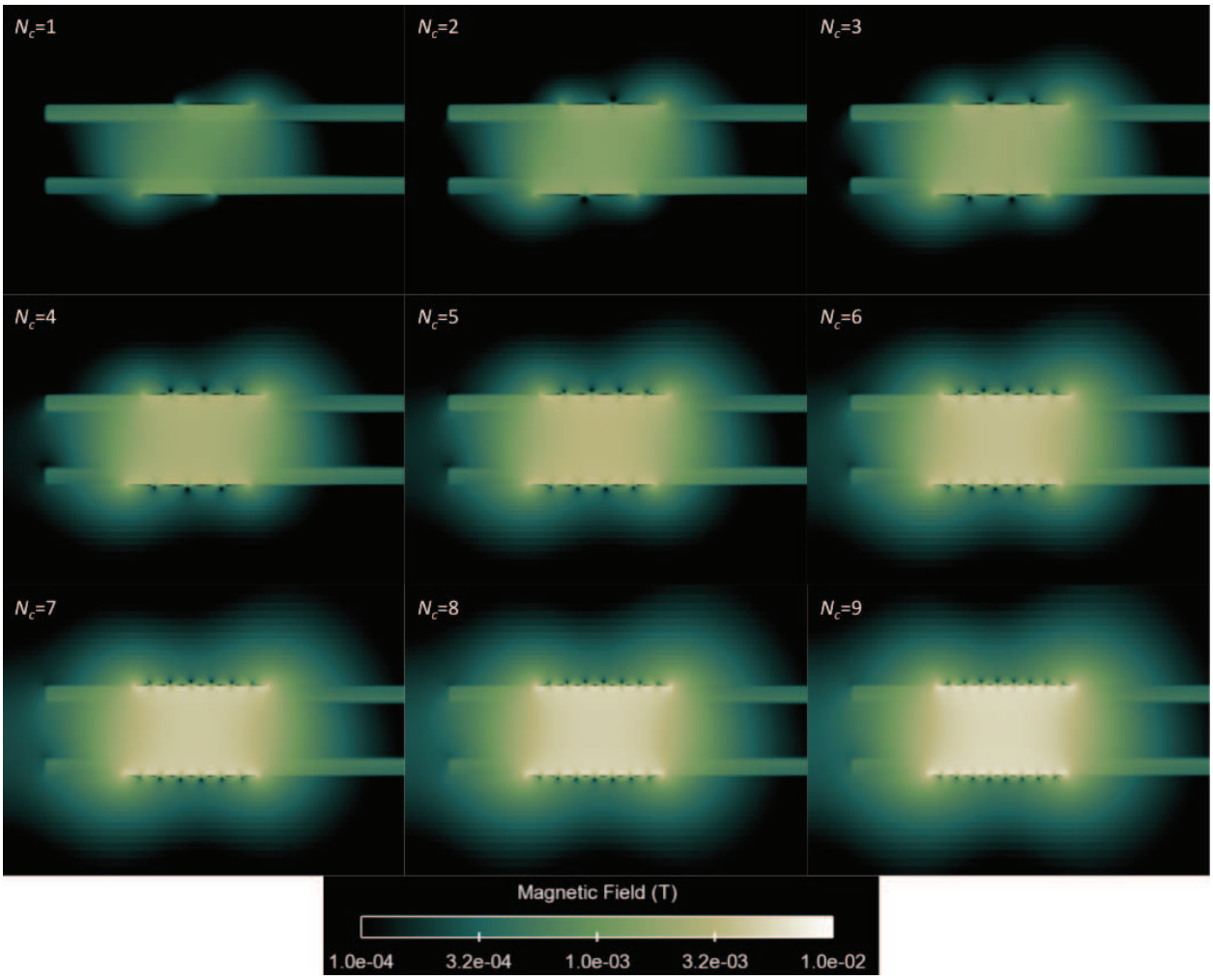

Figure F-1. Helicoil geometries and their associated steady-state magnetic field distribution.

NO. OF COPIES	ORGANIZATION
1 (PDF ONLY)	DEFENSE TECHNICAL INFORMATION CTR DTIC OCA
1	US ARMY RESEARCH LAB RDRL CIO LL
1	GOVT PRINTG OFC A MALHOTRA
1	US ARMY RESEARCH LAB RDRL WMP D R DONEY
2	US ARMY RESEARCH LAB RDRL WMM B G GAZONAS B POWERS
1	US ARMY RESEARCH LAB RDRL WMP S SCHOENFELD
6	US ARMY RESEARCH LAB RDRL WMP A P BERNING C HUMMER A PORWITZKY J POWELL C UHLIG B RINGERS
5	US ARMY RESEARCH LAB RDRL WMP B R BECKER S BILYK S SATAPATHY A SOKOLOW B LEAVY
2	US ARMY RESEARCH LAB RDRL WMP C S SEGLETES T BJERKE
8	US ARMY RESEARCH LAB RDRL WMP D A BARD M KEELE F MURPHY J RUNYEON S SCHRAML G VUNNI M ZELLNER J HOUSKAMP
3	US ARMY RESEARCH LAB RDRL WMP E P BARTKOWSKI D HORNBAKER P SWOBODA
1	US ARMY RESEARCH LAB RDRL WMP F N GNIAZDOWSKI
1	US ARMY RESEARCH LAB RDRL WMP G N ELDREDGE
7	SANDIA NATIONAL LABORATORIES MS 1323 E STRACK J NIEDERHAUS A ROBINSON -MS 1322 C SIEFERT -MS 0380 C GARASI -MS 1189 K COCHRANE T HAILL
1	UNIVERSITY OF ALABAMA AT BIRMINGHAM D LITTLEFIELD
1	DEFENSE RESEARCH AGENCY B JAMES
2	ENIG ASSOCIATES, INC. E ENIG D BENTZ